

Cite this: DOI: 10.1039/xxxxxxxxxx

Supplementary material for: Emission enhancement and polarization of semiconductor quantum dots with nanoimprinted plasmonic cavities: towards scalable fabrication of plasmon-exciton displays

Jasper J. Cadusch,^{a*} Evgeniy Panchenko,^a Nicholas Kirkwood,^b Timothy D. James,^{a,c} Brant C. Gibson,^d Kevin J. Webb,^e Paul Mulvaney,^b and Ann Roberts^a

Received Date
Accepted Date

DOI: 10.1039/xxxxxxxxxx

www.rsc.org/journalname

A quantum dot (QD) display can consist of either a QD cell illuminated from the side by a GaN LED for optical excitation or a metallic contact, typically aluminium, the quantum dot layer and a transparent hole transport layer (such as graphene oxide)¹, with a transparent top contact, usually indium tin oxide (ITO)², for direct electrical excitation. Emission can then be controlled electronically. We propose the metallic contact could be structured with cold forging to cost effectively increase the QD pixel brightness and polarize the emission from each pixel. This would allow for 3D display technology and further reduce the cost and energy consumption of QD displays. The same cold forging techniques can also be readily extended to increase the efficiency of QD based solar cells, although the metasurface response should be polarization independent in this case.

Previously, the spectral response of plasmonic cavities created with RNIL showed surprisingly sharp and short wavelength resonances, compared to apertures of similar dimensions³, with Q factors similar to those of quadrupolar modes of nanoantennas, but with intensities more akin to dipolar modes^{4,5}, as shown in the numerical calculations presented in figure S3(a). These modes have a node of the electric field at the metal-dielectric boundary at one end of the nanocavity. When considering real metals, there is a small length correction to account for the skin

effect due to the metal's finite conductivity. The fundamental cavity mode is similar to the first order Fabry-Perot mode of the equivalent aperture, in a free standing metal film with twice the thickness. A comparison of the resonant modes is shown in figure S3(b-c). Far from being a shortcoming, this fact permits strong blue resonances in nanocavities, something that is critical to color displays, is difficult to achieve with nanoapertures and is a major issue for current OLED based displays.

The geometric dependence of the resonant properties of the nanocavity arrays are shown in Fig. S4. Here we performed finite element method (FEM) calculations of a silver film patterned with a periodic array of nanocavities in air. The cavity width was held fixed at 40 nm and the period at 300 nm, we varied the length and the depth of the cavities and recorded the resonant wavelength (a) and the total reflectivity (b) in each case. As expected the optical properties of the cavities depend strong both on cavity length and the depth. Fig. S4 (b) shows that there is a set of cavity lengths and depths which have a very low reflectivity, which means our cavities are near-perfect absorbers for this set of parameters. The addition of an SU8 superstrate ($n=1.6$) meant that a resonant wavelength in air of $\lambda = 530$ nm was required to give good spectral overlap with our pre-grown QDs. It has previously been shown that increased cavity depth requires exponentially increasing applied imprint pressure⁵. Thus the shallower the depth, the easier it is to imprint. With these restrictions in mind and referring to Fig. S4, we decided on a length of 200 nm and a depth around 50 nm. This combination of parameters gives cavity resonance at the desired wavelength and with near perfect absorption (very low reflectivity).

Figure S5 shows the collected counts from the QD/SU8 sample on a silver film. A 532 nm CW laser was used to pump the

^a School of Physics, The University of Melbourne, Parkville, VIC 3010, Australia; E-mail: jcadusch@student.unimelb.edu.au

^b School of Chemistry and Bio21 Institute, The University of Melbourne, Parkville, VIC 3010, Australia.

^c Melbourne Centre for Nanofabrication (MCN), Australian National Fabrication Facility, Clayton, VIC, 3168, Australia.

^d College of Science, Engineering and Health, RMIT University, Melbourne, VIC, 3001, Australia.

^e School of Electrical and Computer Engineering, Purdue University, West Lafayette, IN, 47907, USA.

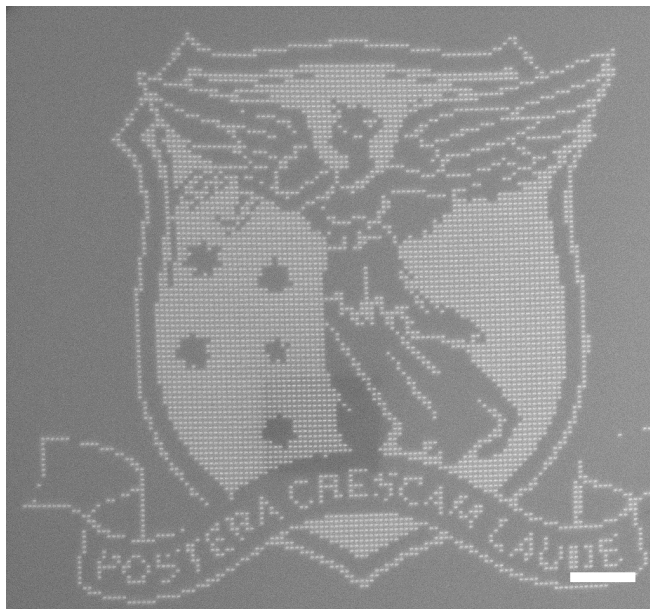


Fig. S1 An SEM image of a HSQ/Si master template, consisting of a structured array of 200 nm by 40 nm nanorods. The white scale bar is 5 μm . The image has been reversed.

QDs through a 0.90 NA 100x Olympus Objective. The objective is mounted on a XYZ piezo stage with a 200 μm scan range in all three directions. The emission was collected through the same lens, passed through a 532 nm dichroic filter into a single-moded optical fiber connected to an avalanche photodiode. The 60 μm core of the optical fiber acts as a pinhole aperture to give the system confocal optical sectioning. By collecting emission at various heights above the silver film and above the nanocavity array, the effect of spectator QDs can be observed. The collected emission from 6 μm above the metallic surface is still 10% of the maximum value. We suspect this effects our lifetime data and our degree of polarization measurements.

By focusing on the silver film and then retracting the objective until QD fluorescence is no longer observed, it is possible to measure the thickness of the SU8 layer. Figure S6 shows the silver surface, with many bright QD aggregates and the same region with the objective 12 μm further away from the sample, where only a few aggregates are visible. Further than 12 μm QD aggregates are no longer visible in the scanned image.

Figure S7 shows the measured spectra for quantum dots near and far from the nanocavity array for the same pump power and collection times. From these spectra we can estimate the increase in external quantum efficiency of the device due to the coupling between cavity plasmons and QD excitons. To do so, we integrate the counts with respect to wavelength for each spectrum and take the ratio. This yields 1.95, or an increase in EQE of 95%.

Figure S8 shows a high resolution transmission electron microscopy (HRTEM) image of the QDs used in this experiment. The sample shows low dispersion in QD size, which leads to narrow emission bands for the QD/SU8 mixture. This also helps reduce the spread in decay rates of our QDs.

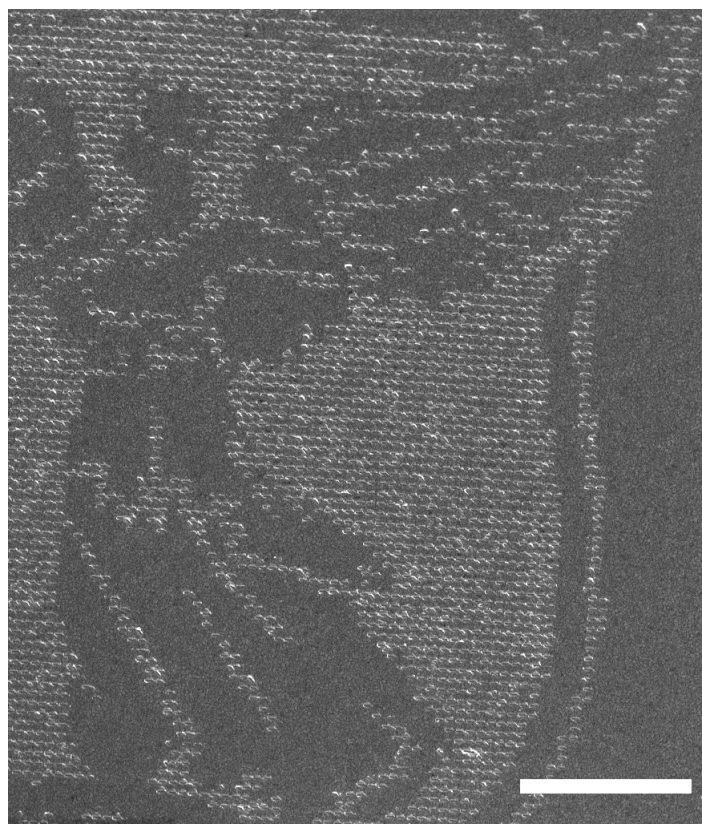


Fig. S2 An SEM image of the imprint in a silver film produced using the master shown in Fig. S1. Note the fine details are made up of only a few nanocavities. The white scale bar is 5 μm

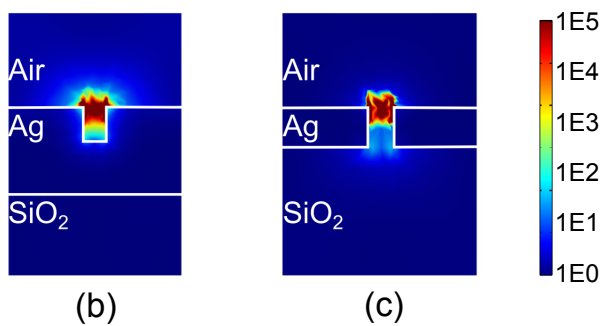
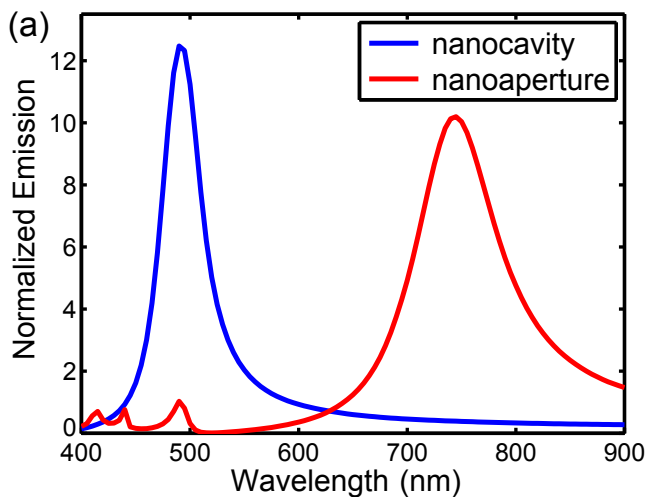


Fig. S3 A comparison of a nanoimprinted metasurface of cavities, and an array of nanoapertures. Both the cavity and the aperture have dimensions of 150 nm x 50 nm x 60 nm, with an array period of 300 nm. The plasmon resonances are driven by a dipole point-source at the center of the entrance of the cavity/aperture. (a) Calculated emission spectra for the point source driven nanocavities (blue) and nanoapertures (red). (b) The electric field strength at resonance for the nanocavities. (c) The electric field strength at resonance for the nanoapertures.

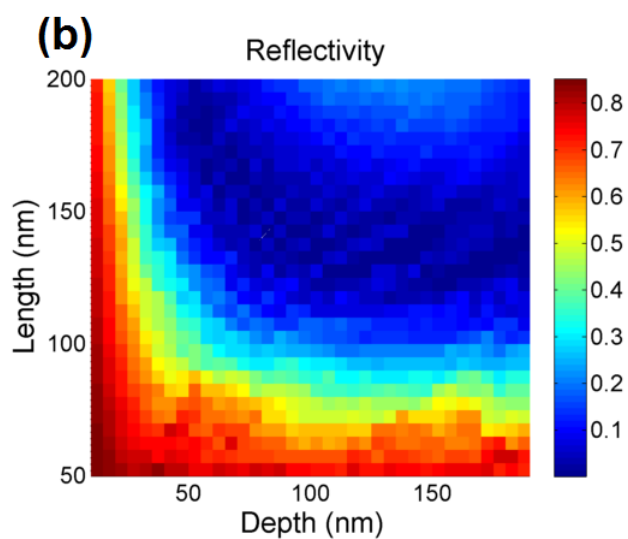
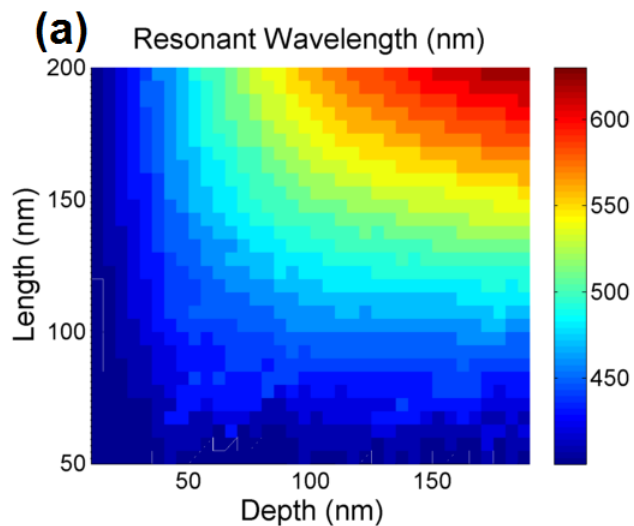


Fig. S4 Calculated cavity resonance wavelengths (a) of a nanoimprinted silver film for a range of cavity lengths and depths and their reflectivity (b).

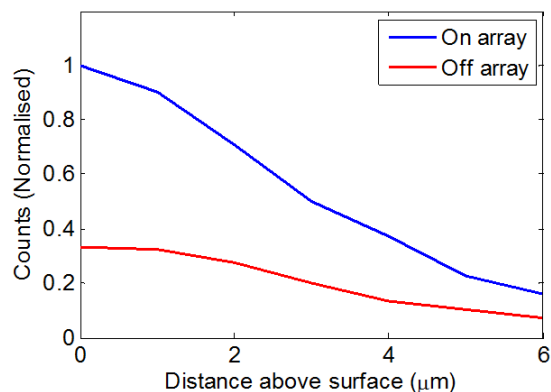


Fig. S5 A comparison of the collected fluorescence from the QDs above the cavity array (blue) and above the unpatterned film (red).

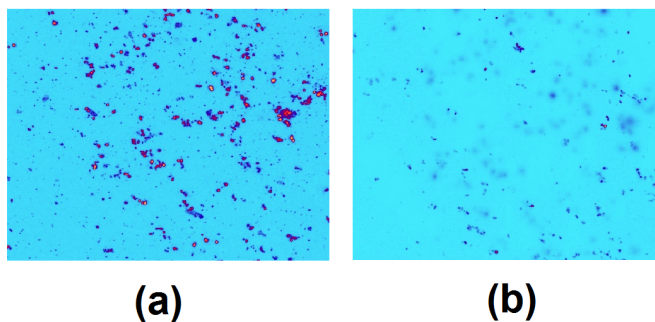


Fig. S6 Confocal scans of the QD/SU8 mixture on the unpatterned silver film, (a) at the silver surface and (b) 12 μm from the silver surface.

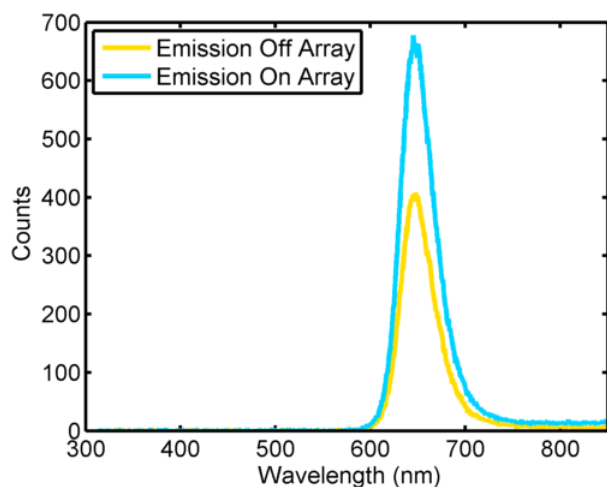


Fig. S7 Spectra from QDs on the cavities (blue) and on the unpatterned silver (yellow). The presence of the cavities increases the EQE by 95%.

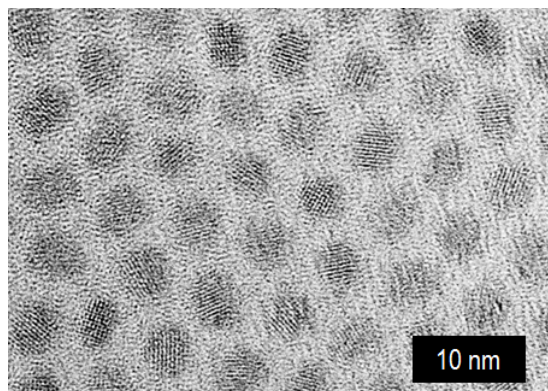


Fig. S8 A HRTEM image of the monodisperse graded alloy shell QDs.

References

- 1 S.-S. Li, K.-H. Tu, C.-C. Lin, C.-W. Chen and M. Chhowalla, *ACS nano*, 2010, 4, 3169–3174.
- 2 T.-H. Kim, K.-S. Cho, E. K. Lee, S. J. Lee, J. Chae, J. W. Kim, D. H. Kim, J.-Y. Kwon, G. Amaratunga, S. Y. Lee *et al.*, *Nature Photonics*, 2011, 5, 176–182.
- 3 J. J. Cadusch, T. D. James and A. Roberts, *Optics Express*, 2013, 21, 28450–28455.
- 4 S. Kim, Y. Xuan, V. P. Drachev, L. T. Varghese, L. Fan, M. Qi and K. J. Webb, *Optics Express*, 2013, 21, 15081–15089.
- 5 L. T. Varghese, L. Fan, Y. Xuan, C. Tansarawiput, S. Kim and M. Qi, *Small*, 2013, 9, 3778–3783.